

# communications materials

## ARTICLE

<https://doi.org/10.1038/s43246-021-00128-z>

OPEN



## Atomic resolution imaging of cation ordering in niobium-tungsten complex oxides

Sumio Iijima<sup>1</sup> <sup>1</sup>✉, Wenhui Yang<sup>2</sup>, Syo Matsumura<sup>2</sup> & Ichiro Ohnishi<sup>3</sup>

Energy dispersive X-ray emission imaging at atomic resolution is a powerful tool to solve order-disorder problems in complex metal oxide crystals, supplementing conventional X-ray or neutron diffraction. Here, we use this method, based on scanning transmission electron microscopy, to investigate cation ordering in ternary metal oxides  $4\text{Nb}_2\text{O}_5\cdot 9\text{WO}_3$  and  $2\text{Nb}_2\text{O}_5\cdot 7\text{WO}_3$ , which have recently attracted attention as energy storage materials in lithium-ion batteries. Their crystal structures are a tetragonal tungsten bronze-type and its hybrid with a  $\text{ReO}_3$ -type ‘block structure’, respectively. Our study reveals the presence of chemical ordering of metal ions in these materials, which have previously been assumed to be solid-solutions. In particular, we show that the two types of cations, Nb and W, are well ordered in their lattices, and that the Nb ions tend to occupy one third of the pentagonal channel sites. These results demonstrate that atomic resolution X-ray emission imaging is an effective alternative approach for the study of locally ordered crystal structures.

<sup>1</sup> Meijo University, Graduate School of Science and Technology, Nagoya, Japan. <sup>2</sup> Kyushu University, Department of Applied Quantum Physics and Nuclear Engineering, Fukuoka, Japan. <sup>3</sup> JEOL Ltd., Tokyo, Japan. ✉email: [iijimas@meijo-u.ac.jp](mailto:iijimas@meijo-u.ac.jp)

In materials science, it is essential to determine the true crystal structure of materials, so that their functionalities may be understood and optimised for application purposes. Traditionally, crystal structures are examined by X-ray or neutron diffraction methods, but these provide only an averaged structure and no local one. Transmission electron microscopy (TEM), however, has been covering the weakness of the diffraction methods. As the resolving power of the microscope improved, it has been possible to image individual atoms or columns of atoms in a crystal<sup>1,2</sup>. Simultaneously, its peripheral devices such as electron energy loss spectroscopy (EELS) and energy-dispersive X-ray spectroscopy (EDS) have been developed. As a result, a modern scanning TEM (STEM) technique with aberration correction combined with EELS<sup>3</sup> or EDS is widely used now to investigate the elemental distribution or mapping of a crystal at the atomic resolution. The first atomic-resolution EDS study of a single atom was performed by Suenaga et al.<sup>4</sup>, who detected an EDS L-line signal from a single Er atom embedded into a single-walled carbon nanotube. Utilising the atomic resolution A STEM-EDS imaging system, Shibata et al.<sup>5</sup>, studied the segregation of dopant atoms at ceramic grain boundaries<sup>6</sup>. Atomic resolution EDS imaging of ordered precipitations in metal alloys was also reported by Holmestad et al.<sup>7</sup> and other groups<sup>8</sup>.

Nb–W oxide systems are of interest for possible application in energy storage materials, such as lithium-ion batteries<sup>9,10</sup>. The crystal structures of these oxides contain open channels of trigonal, square, and pentagonal rings of metal oxygen-octahedra (denoted  $MO_6$ ) that go along the  $c$ -axis. These channels are expected to contribute to ion transport for lithium ions<sup>9</sup>. Furthermore, the constituting metal atoms, Nb and W, are multivalent ions, and, therefore, the oxides have ambiguous stoichiometry, suggesting that they might have crystalline defects and some types of the cation ordering<sup>11,12</sup>. Such information on the local crystal structures is important in practical applications. Interestingly, most researchers working on practical energy storage applications have not paid attention to these local crystal structures<sup>9,10,13</sup>.

In the present study, STEM-EDS electron microscopy was applied to understand cation ordering in two Nb–W oxide systems,  $4Nb_2O_5\cdot 9WO_3$  (hereafter 4:9) and  $2Nb_2O_5\cdot 7WO_3$  (hereafter 2:7). These crystals are available in powder form; therefore, the conventional X-ray powder diffraction methods that are typically used for crystal structure analysis are insufficient for distinguishing between different metal ion sites. This issue has been partially supplemented by a Rietveld powder neutron diffraction method<sup>14</sup>. The 4:9 and 2:7 crystals were examined to determine their metal ion orderings via elemental mapping. Both crystals have a basic structure of the tetragonal tungsten bronze (TTB)<sup>15,16</sup>, and the latter compound possesses a mixture of TTB and  $ReO_3$ -type structures<sup>17,18</sup>. A common structural unit of these crystals consists of a metal–oxygen octahedron (denoted  $MO_6$ ) connected to the neighbouring octahedra through their corners to form a two-dimensional network. To construct a three-dimensional structure, multiple two-dimensional networks are stacked along the  $c$ -axis at a distance equal to the octahedron diagonal (0.38 nm). The described oxide crystals were synthesised via a solid-state reaction between  $WO_3$  and  $Nb_2O_5$  powders. The former reagent had a  $ReO_3$ -type structure, and the latter possessed a so-called “block structure” that was composed of small  $ReO_3$  blocks connected via shared corners and edges.

Our study reveals that the two types of cations, Nb and W, are well ordered in their lattices and that the Nb ions tend to occupy one-third of the pentagonal channel sites. Importantly, we believe that the herein illustrated atomic resolution X-ray emission imaging method will represent a useful and alternative approach in the various fields concerning crystallography.

## Results and discussion

**STEM-EDS imaging of  $2Nb_2O_5\cdot 7WO_3$  crystals.** The Nb–W–O ternary oxide system examined in this study had a nominal composition of  $19Nb_2O_5\cdot 63WO_3$  that corresponded to the oxygen–metal ratio O/M ( $M = Nb$  or  $W$ ) of 2.811. Two different crystal structures of  $Nb_2O_5\cdot WO_3$  (2:7 and 4:9) exist in this compositional range. The first structure was the dominant phase with an O/M ratio of 2.818, which was close to the nominal composition of 2.811<sup>17</sup>. The second phase had an O/M ratio of 2.765 and is described in more detail in the next section<sup>18</sup>.

The XRD work of the studied compound oxide was reported elsewhere<sup>19</sup>; it has been also cited in a recent investigation of an energy storage material<sup>9</sup>. However, its revised structure has been published by one of the authors in early works devoted to high-resolution electron microscopy<sup>18</sup>. The crystal structure of 2:7 contains intergrown TTB-type and  $ReO_3$ -type lattices with the crystal space group  $P4$ . Its model is shown in Fig. 1a, where the blue squares represent the metal–oxygen octahedra  $MO_6$  connected through their corners to form a network that is stacked along the  $c$ -axis direction ( $c = 0.3924$  nm). This structure is basically composed of  $2 \times 2$  TTB-type units ( $a = b = 2.426$  nm), and its central region contains a  $4 \times 4$  slab of  $ReO_3$ -type octahedra. It also includes three different types of tunnels (trigonal, square, and pentagonal ones), and some of the pentagonal tunnels are regularly occupied with metal–oxygen ( $MO$ ) chains denoted by the red balls. The electron diffraction pattern of the  $a^*b^*$  reciprocal lattice section depicted in Fig. 1b confirms the tetragonal  $P4$  symmetry. The diffraction spots with slightly higher intensities displayed at the square corners originated from the  $ReO_3$ -type region coherently intergrown into the TTB-type lattice (Fig. 1a).

The STEM high angle dark field (HAADF) image of the oxide crystal is shown in Fig. 1c. It was taken by scattering electron waves in the high-angle regions. As a result, metal atoms were imaged more distinctly as the white blobs, while no lighter elements (such as oxygen atoms) were detected. The coordinates of the metal atoms obtained directly from the image as well as the estimated coordinates of the oxygen atoms are listed in Table 1.

Figure 1d shows the overlay image of the two STEM-EDS images of the region depicted in Fig. 1c that were recorded using the Nb La X-ray emission and W Ma emission lines. The wide views of the original Nb La and W Ma EDS images, as well as the HAADF image, are displayed in Fig. 2. Here, the green blobs denote the Nb-dominant sites and the red ones—the W-dominant sites. From the obtained data, it can be concluded that the brightest green blobs populate regularly one-third of the pentagonal tunnels occupied by  $MO$  chains (see the red balls in Fig. 1a), indicating that these tunnels are mainly filled with Nb ions (Fig. 2c). In contrast, the red blobs are located in the central region of the unit cell with the  $ReO_3$ -type octahedral structure predominantly occupied by W ions (see also Fig. 2b). The brightness values of both the green and red balls differ at various metal ion sites reflecting the occupancies of Nb and W ions, respectively.

The semiquantitative occupancies of the metal ion sites determined from the images depicted in Fig. 2 are tabulated in Table 2 (note that these values are not absolute but relative occupancies of metal atoms). The brightest green blobs were found to be occupied by Nb ions (71%) and W ions (29%). Similarly, the highest occupancy of W ions equal to 74% was obtained for the octahedral sites located in the centre of the  $ReO_3$  region. The ordering of metal ions in the 2:7 crystal will be discussed in the next section.

**STEM-EDS imaging of  $4Nb_2O_5\cdot 9WO_3$  crystals.** The most likely ordering of metal ions was also determined for the 4:9 crystal with

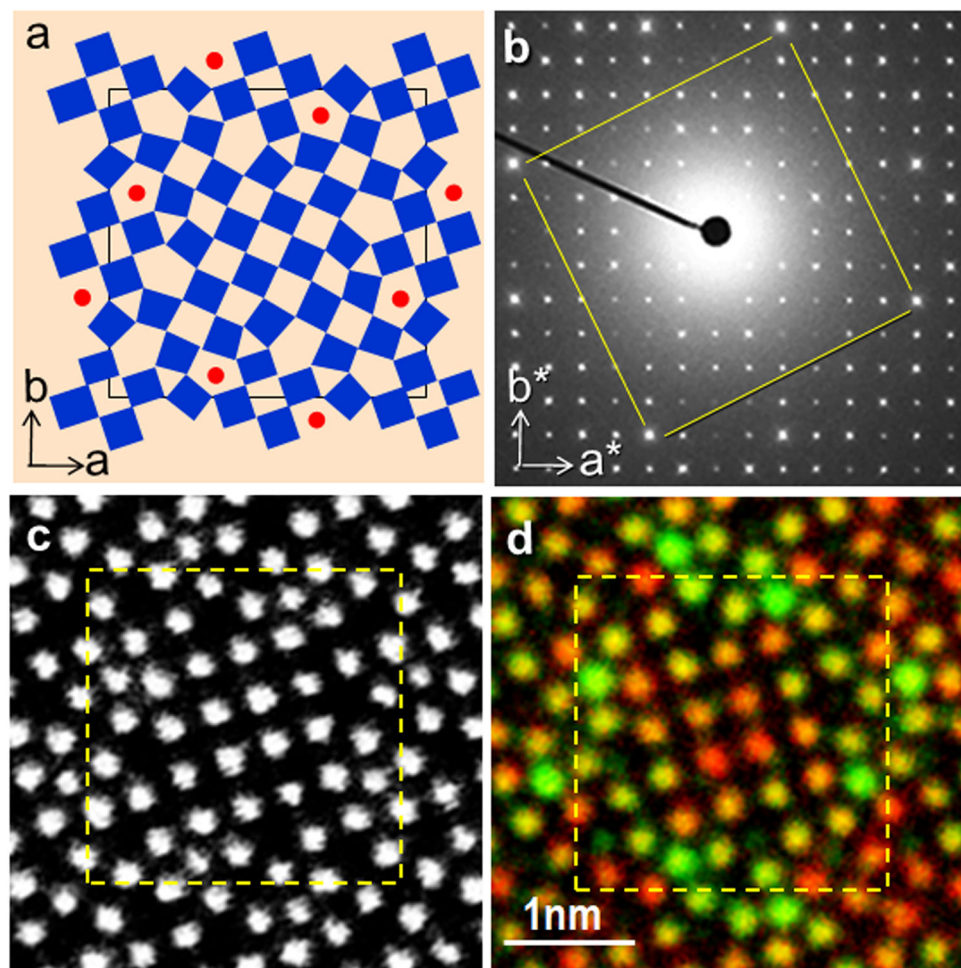


**Fig. 1 Atomic resolution STEM-EDS imaging of a crystal of  $2\text{Nb}_2\text{O}_5\cdot 7\text{WO}_3$  oxides.** **a** A schematic model of the  $2\text{Nb}_2\text{O}_5\cdot 7\text{WO}_3$  crystal. **b** An electron diffraction pattern obtained for the thin chip of the  $2\text{Nb}_2\text{O}_5\cdot 7\text{WO}_3$  crystal oriented in the [001] direction parallel to the incident electron beam. **c** A HAADF-STEM image showing the individual metal atom columns (white blobs) of the  $2\text{Nb}_2\text{O}_5\cdot 7\text{WO}_3$  crystal with the orientation specified in panel (b). **d** A STEM-EDS image of the overlaid crystal images recorded using the Nb La X-ray (green) and W Ma X-ray (red) lines (see Fig. 2b, c, respectively), which corresponds to the image depicted in panel (c). The crystal unit cell is indicated by the square.

an O/M ratio of 2.765. The crystal was found as a minor phase in the presently examined specimen with the nominal composition of 2.811. Its orthorhombic structure consisting of  $1 \times 3$  TTB-type units is very similar to the 2:7 structure and contains trigonal, square, and pentagonal tunnels (Fig. 3a). Four out of twelve pentagonal tunnels are occupied by MO chains (blue arrows). According to the results of XRD analysis, Nb and W ions appear to be disordered; however, the R-factor was slightly improved by weighting the Nb ions in the pentagonal channels<sup>15</sup>.

The metal ion sites (octahedra) are clearly visible in the image recorded in the STEM-HAADF mode (Fig. 3b). Here, oxygen ions are not visualised because of their low electron scattering intensities but they became visible in the STEM annular bright field imaging mode<sup>20</sup>. The two STEM-EDS images obtained using the W Ma X-ray emission (pink) and Nb La emission (yellow) lines are shown in Fig. 3c, d, respectively. Both images were trimmed to exactly match the HAADF image; therefore, the metal atom sites depicted in Fig. 3b show a good one-to-one correspondence with those in the EDS images. However, some metal atoms appear to be missing (such as the ones indicated by the yellow arrows in the W Ma image (Fig. 3c)); however, these sites are visualised as the brightest yellow blobs in the Nb La image (Fig. 3d), corresponding to the Nb ions with the highest occupancies. The regular arrangement of these ions is confirmed

by the wide Nb La image shown in Fig. 4c. The images depicted in Fig. 4 indicate that the Nb ions in the 4:9 crystal are periodically arranged in the pentagonal tunnels (in other words, the Nb ions in the 4:9 structure are highly ordered). The preferential occupancies of the metal sites listed in Table 2 will be discussed below.

**Chemical orderings of cations in TTB-type complex metal oxide crystals.** The ternary transition metal oxide systems studied in this work include multivalent Nb and W ions ( $\text{Nb}^{5+}$ ,  $\text{Nb}^{4+}$ ,  $\text{Nb}^{3+}$ ,  $\text{W}^{6+}$ , and  $\text{W}^{5+}$ ) with different coordination numbers. The W ions with six valence electrons likely form a  $\text{MO}_6$  octahedron with a coordination number equal to six, and almost all metal ions in the studied oxides are situated in  $\text{MO}_6$  octahedra. In addition, pentagonal bipyramids  $\text{MO}_7$  with a coordination number of seven are formed only by the MO chains located at the pentagonal tunnel sites.

Metal occupancy is represented by various colours from green (Nb) to red (W), and the occupancy ratios Nb/Nb + W measured for the 11 crystallographically independent metal ion sites in the 2:7 crystal and labelled by numbers from 1 to 11 in Fig. 4a-c are listed in Table 1. The same number indicates crystallographically equivalent sites. For example, the #1 sites are the Nb-dominant

**Table 1** Atomic coordinates in the 2:7 crystal deduced from the HAADF image depicted in Fig. 1b.

Atom	Nb occupancy	x	y	z	Atom	Occupancy	x	y	z
M1	0.71	0.341	0.068	0.5	O22	1.0	0.037	0.083	0
M2	0.60	0.041	0.388	0.5	O23	1.0	0.016	0.156	0
M3	0.36	0.353	0.202	0.5	O24	1.0	0.017	0.322	0
M4	0.44	0.097	0.033	0.5	O25	1.0	0.242	0.056	0
M5	0.50	0.468	0.088	0.5	O26	1.0	0.142	0.098	0
M6	0.37	0.217	0.132	0.5	O27	1.0	0.168	0.199	0
M7	0.46	0.152	0.284	0.5	O28	1.0	0.297	0.154	0
M8	0.37	0.021	0.240	0.5	O29	1.0	0.402	0.137	0
M9	0.38	0.492	0.257	0.5	O30	1.0	0.421	0.023	0
M10	0.49	0.299	0.346	0.5	O31	1.0	0.498	0.162	0
M11	0.26	0.446	0.385	0.5	O32	1.0	0.429	0.222	0
O12	1.0	0.097	0.033	0.5	O33	1.0	0.332	0.278	0
O13	1.0	0.021	0.240	0.5	O34	1.0	0.221	0.332	0
O14	1.0	0.217	0.132	0.5	O35	1.0	0.110	0.350	0
O15	1.0	0.468	0.088	0.5	O36	1.0	0.091	0.240	0
O16	1.0	0.353	0.202	0.5	O37	1.0	0.091	0.447	0
O17	1.0	0.152	0.284	0.5	O38	1.0	0.261	0.414	0
O18	1.0	0.041	0.388	0.5	O39	1.0	0.375	0.362	0
O19	1.0	0.492	0.257	0.5	O40	1.0	0.466	0.318	0
O20	1.0	0.299	0.346	0.5	O41	1.0	0.426	0.458	0
O21	1.0	0.446	0.385	0.5	O42	1.0	0.341	0.068	0.5

The Nb/(Nb + W) metal occupancies were obtained from the STEM-EDS images presented in Fig. 2.

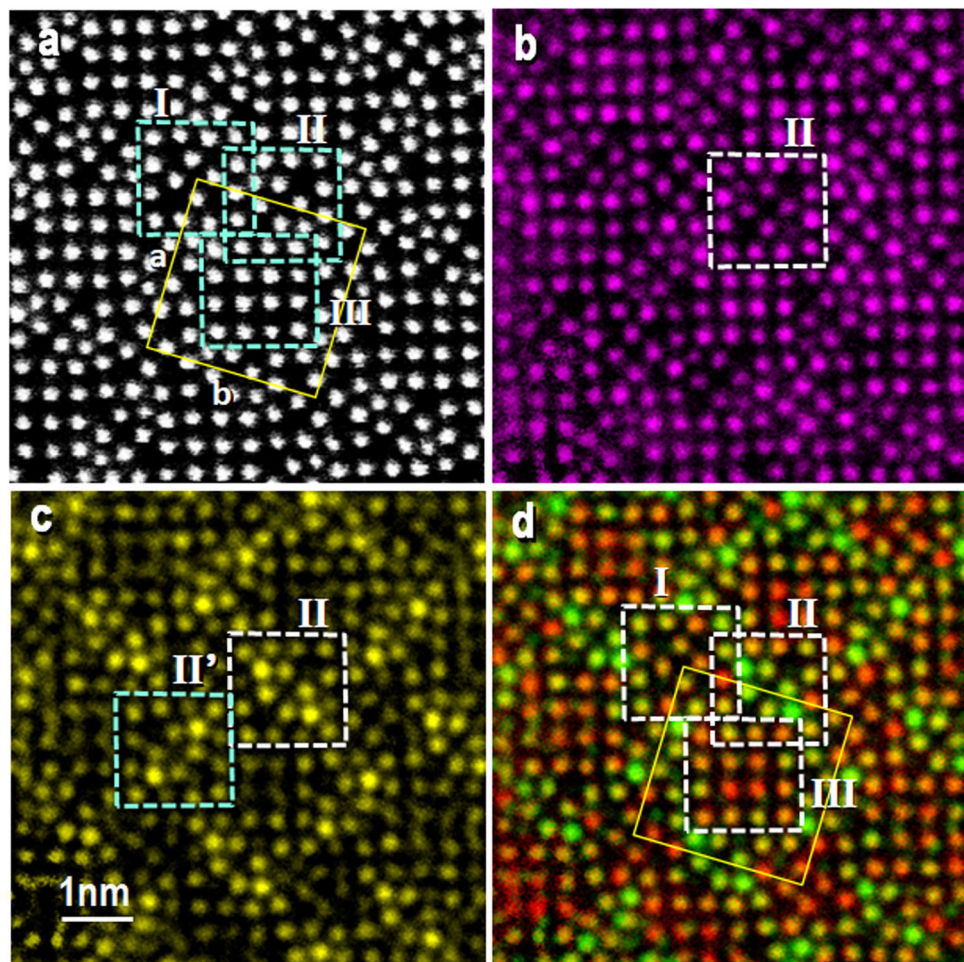


**Fig. 2** Atomic resolution STEM images recorded for the same region of the  $2\text{Nb}_2\text{O}_5\cdot 7\text{WO}_3$  crystal. The blobs denote the individual metal–oxygen atomic columns oriented perpendicularly to the page. The unit cell is indicated by the square. **a** A HAADF image. STEM-EDS images recorded using the **b** W M $\alpha$  (pink) and **c** Nb L $\alpha$  (yellow) X-ray emission lines. **d** An overlay image of the two W and Nb X-ray emission images depicted in panels **(b)** and **(c)**, respectively. The dotted squares show the TTB-type structure unit or the  $\text{ReO}_3$  type.

**Table 2** Metal ion occupancies determined for crystals  $2\text{Nb}_2\text{O}_5\cdot7\text{WO}_3$  and  $4\text{Nb}_2\text{O}_5\cdot9\text{WO}_3$ .

Metal occupancies (Nb/W + Nb)											
Atom	M1	M2	M3	M4	M5	M6	M7	M8	M9	M10	M11
Sample											
2:7	0.71	0.60	0.36	0.44	0.50	0.37	0.46	0.37	0.38	0.49	0.26
4:9	0.78	0.43	0.34	0.33	0.42	0.36	0.38	0.23	0.31		

Note the values are not absolute but relative occupancies.

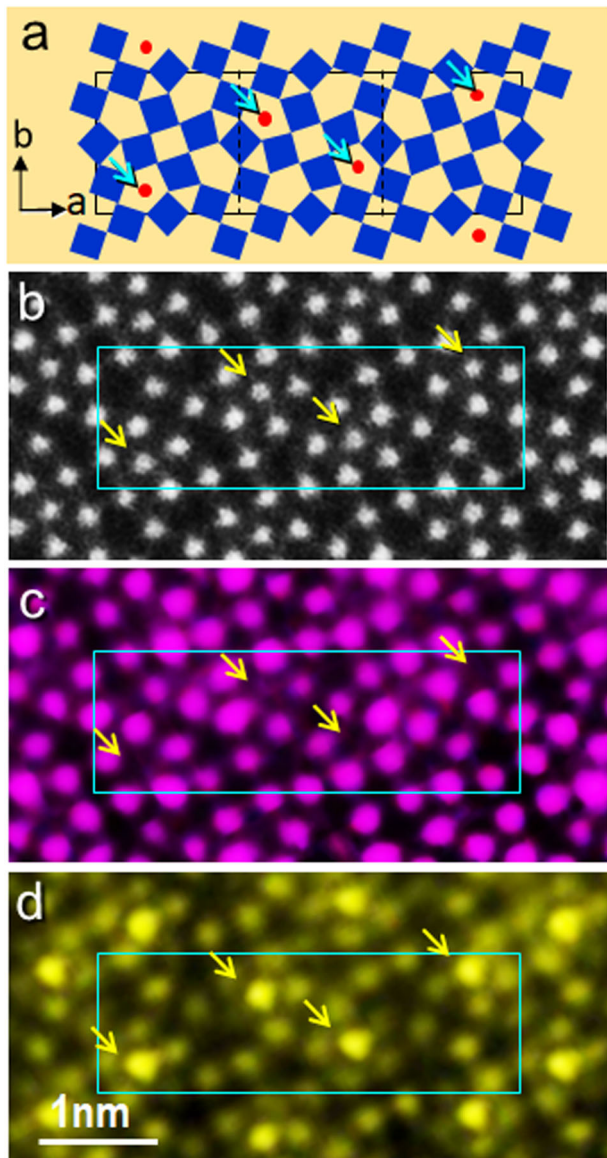


**Fig. 3** Atomic resolution STEM-EDS imaging of a crystal of  $4\text{Nb}_2\text{O}_5\cdot9\text{WO}_3$  oxides. **a** A schematic model of the  $4\text{Nb}_2\text{O}_5\cdot9\text{WO}_3$  crystal. **b** A HAADF-STEM image showing the individual metal atom columns (white blobs) of the crystal oriented in the [001] direction with respect to the incident electron beam. STEM-EDS images recorded using the **c** W Mo X-ray (pink) and **d** Nb La X-ray (yellow) lines. All images in panels **(a)**–**(c)** were obtained for the same crystal area. The arrows indicate the metal atom columns located in the pentagonal tunnels of the crystal structure. The image intensities of the tunnels in panel **(c)** are close to zero; however, the corresponding values obtained in panel **(d)** are very high, suggesting that these sites are predominantly occupied by Nb atoms.

sites with the darkest green colour (occupancy: 0.71), and the #11 sites are the red-coloured W dominant sites (occupancy: 0.26). The four #4 sites are represented by the lighter red colour and have a prevalent Nb population with an occupancy of 0.44. As we discuss later, nearly 70% of the Nb ion occupancy in the 4:9 crystal was obtained for its #1 sites (Fig. 4d). It should be noted that the occupancies are always a fraction of 100% within a MO column, meaning that the Nb and W ions are distributed randomly or in some kinds of ordering within the column. In the present experiment, we did not examine the existence of such orderings in the *c*-axis direction. For this reason, strictly speaking, the ordering used in the present paper should be partial ordering.

First, let us consider the local symmetries of the 2:7 crystal structure. The structure can be divided into three regions enclosed by the white dotted squares and labelled I–III in Fig. 2d (their enlarged images are shown in Fig. 5a–c, respectively). Region I contains a TTB-type structure with four open pentagonal tunnels (Fig. 4a). Region II has the same TTB-type structure, except that two out of its four pentagonal tunnels are mainly filled with Nb–O chains, as shown in Fig. 5b, f. The Nb ion in the  $\text{MO}_7$  structure with a coordination number of seven is bonded to the five nearest-neighbouring oxygen ions located on the *ab* plane and two oxygen ions on its top and bottom along the *c*-axis direction. Region III is located at the centre of the unit cell and contains the  $\text{ReO}_3$ -type slab with  $4 \times 4$  octahedra (Fig. 5c), as shown in Fig. 5e.

Note that if we focus only on the positions of the ions in region II and ignore their colours, they form two diagonal mirror planes (Fig. 5b). However, after taking the ion colours into account, the mirror symmetry is transformed into a twofold rotation symmetry (e.g., see two #8 sites). In other words, the twofold rotation symmetry likely originates from the different occupancies of Nb and W ions. Let us now use the same approach for the analyses of regions I (Fig. 5a) and III (Fig. 5c). Both of them apparently exhibit four mirror symmetries near the centres. However, they actually possess only the fourfold rotational symmetry for the reason mentioned above. It is noteworthy that the TTB-type units with the twofold rotational symmetry are oriented in two directions, as shown by squares II and II' in Fig. 2c, while the I and III units can coexist uniquely at the fourfold rotational symmetry centre of the 2:7 crystal unit cell. These symmetry elements apparently form the crystal space group  $P4$ .

The ordering of Nb and W ions was also confirmed for the 4:9 structure composed of  $1 \times 3$  TTB units (Fig. 4). The TTB unit in the middle of the unit cell is shown in Fig. 5d, which corresponds to the region indicated by the dotted square II in the overlay image obtained using the W Mo emission and Nb La emission lines (Fig. 4d). Note that this TTB unit has two orientations indicated by squares II and II' in Fig. 4c. This image is almost identical to that obtained for the 2:7 crystal (Fig. 5b, f). Here, the Nb pentagonal sites labelled #1 (yellow) and W ion sites labelled #8 (pink) have the highest occupancies. Furthermore, the metal ion occupancy determined for each octahedron with the

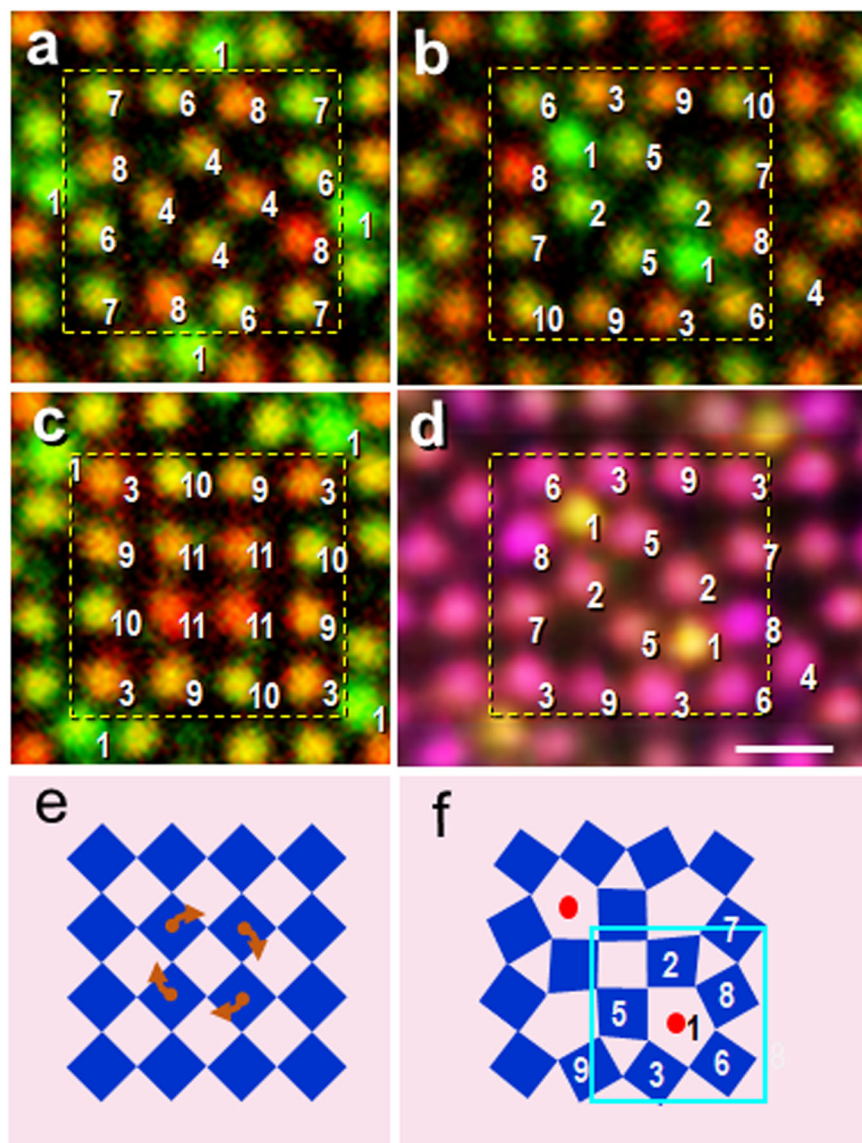


**Fig. 4 Atomic resolution STEM images recorded for the same region of the  $4\text{Nb}_2\text{O}_5\cdot9\text{WO}_3$  crystal.** The blobs denote the individual metal–oxygen atomic columns oriented perpendicularly to the page. The unit cell is indicated by the rectangle. **a** A HAADF image. STEM-EDS images recorded using the **b** W  $\text{M}\alpha$  (pink) and **c** Nb  $\text{L}\alpha$  (yellow) X-ray emission lines. **d** An overlay image of the two W and Nb X-ray emission images depicted in panels **(b)** and **(c)**, respectively. The dotted line squares denote the TTB-type units with two orientations (II and II').

five octahedral sites surrounding the pentagonal tunnels is nearly identical to those obtained for the 2:7 crystals (see Fig. 5b). The occupancies of these metal sites are listed in Table 2. For example, the Nb-richest ion sites #1 in both structures are accompanied by the W-richest ion sites #3 and #8, respectively. Comparing the two images (Fig. 5b, d), it can be concluded that the arrangements of Nb and W ions in both oxides, as well as their twofold rotational symmetries, appear to be the same.

**Cation ordering and structural modifications in the TTB-type structure.** It was found that one-third of the pentagonal tunnels in both the 2:7 and 4:9 crystals were occupied predominantly with Nb ions in a regular fashion, (see Figs. 2 and 4, respectively). The crystal structure of the 4:9 crystal is composed of only one type of TTB structural units oriented in two different directions, as indicated by squares II and II' in Fig. 4c. Two out of the four pentagonal tunnels in the TTB unit (highlighted by the dotted squares in Fig. 4d) are filled with Nb–O chains. Interestingly, the same phenomenon was also observed for the 2:7 crystal (Fig. 5b).

However, this crystal contains another type of TTB units with four open tunnels (Fig. 5a). Note that not more than three out of the four pentagonal tunnels in the TTB units of the studied oxide crystals with the nominal composition  $19\text{Nb}_2\text{O}_5\cdot63\text{WO}_3$  (M/O ratio: 2.811) have ever been filled simultaneously. However, recently a TTB unit having three occupied tunnels was reported for the  $9\text{Nb}_2\text{O}_5\cdot16\text{WO}_3$  compound with a M/O ratio of 2.735, which was close to the M/O ratio 2.765 of the 4:9 crystal discussed here<sup>18</sup>.

One of the interesting observations made in the present study is that the two metal ion sites #1 and #8 that are predominantly occupied by Nb and W ions, respectively, always appear in pairs in the TTB units of both the 4:9 and 2:7 crystals. The STEM-EDS images of such units (containing fully open and two filled pentagons) are reproduced in Fig. 5a, b. A close examination of these images revealed the existence of three types of pentagonal tunnel shapes indicated by letters A, B, and C in Fig. 6c. The pentagon of the five octahedra forming tunnels A is a deformed regular pentagon that is present in pentagonal tunnels B and C.

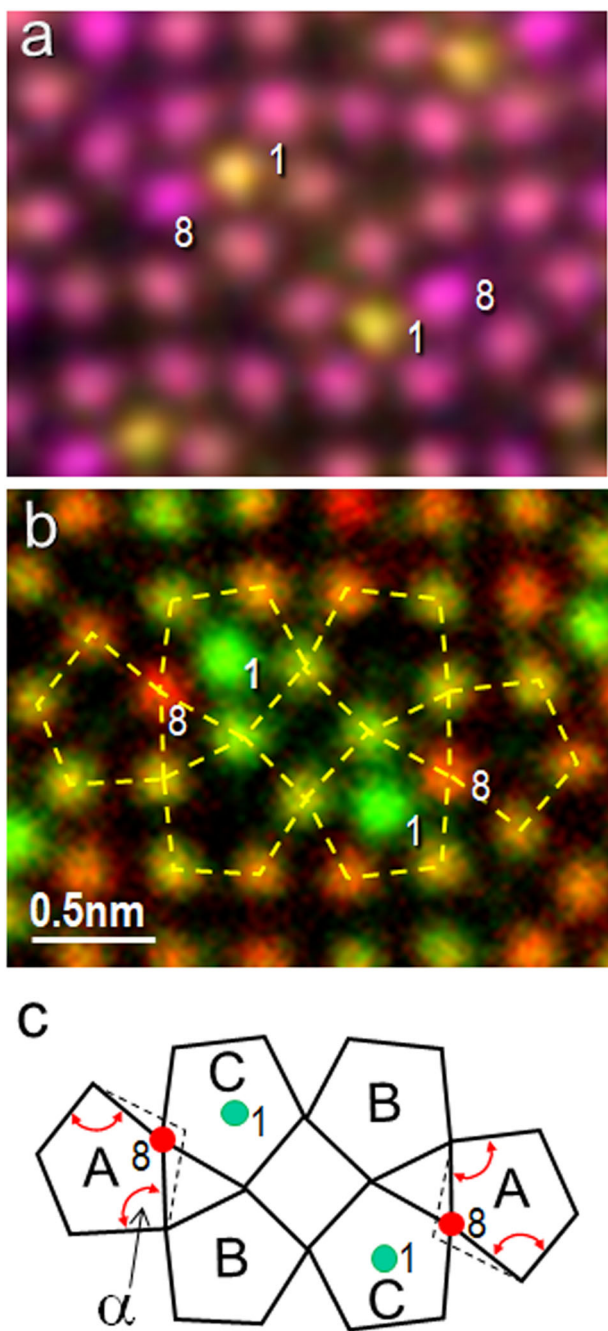


**Fig. 5 STEM-EDS observations on atomic resolution cation occupancies at the various metal–oxygen octahedral sites for the crystals of  $2\text{Nb}_2\text{O}_5\cdot7\text{WO}_3$  and  $4\text{Nb}_2\text{O}_5\cdot9\text{WO}_3$  oxides.** Three regions of the overlay STEM-EDS image of the  $2\text{Nb}_2\text{O}_5\cdot7\text{WO}_3$  crystal structure depicted in Fig. 2d and reproduced in panels (a–c). They are enclosed by the dotted line squares I–III, respectively. **a** Region I containing the TTB structure with four empty pentagonal tunnels. The integer numbers on each blob denote the crystallographically equivalent metal ion sites. **b** Region II similar to that depicted in panel (a), in which two pentagonal tunnels are primarily occupied with Nb–O chains; its illustration is shown in panel (f). **c** Region III with the  $\text{ReO}_3$ -type structure depicted in panel (e). The metal occupancy ratios measured for these regions are listed in Table 2. **d** A STEM-EDS image of a part of the  $4\text{Nb}_2\text{O}_5\cdot9\text{WO}_3$  crystal unit cell, whose structural components are almost identical to those of the  $2\text{Nb}_2\text{O}_5\cdot7\text{WO}_3$  crystal depicted in panel (b). The scale bar is 0.5 nm.

This deformation was caused by the shift of #8 ion sites toward the pentagon centre indicated by the dotted lines. It was also confirmed by one of the pentagon interior angles ( $\alpha$ ) equal to approximately  $90^\circ$ .

The observed shift of #8 octahedra toward the pentagon centre can be related to the presence of the #1 octahedra paired with the former ones. Although we have not specified oxygen ion sites in this study, their positions can be identified from the shapes of the pentagonal rings. In other words, the metal–oxygen bond lengths determined for #1 ions are almost the same because of the nearly regular pentagonal ring shapes (Fig. 6a, b). On the contrary, the metal–oxygen octahedra in the deformed pentagonal rings can be deformed as well. In particular, the metal–oxygen bond length in #8 ions would be shorter than those in the other ions. This deformation of pentagonal rings is likely related to the valences and occupations of the metal ions at the Nb-rich #1 and W-rich #8 sites. The stable atomic structures of these oxide crystals should be considered during the estimations of their energies via density-functional theory calculations.

**Solid-state reaction.** The complex oxide crystals studied in this work were synthesised by a solid-state reaction between  $\text{Nb}_2\text{O}_5$  and  $\text{WO}_3$  powders. The basic crystal structure of  $\text{Nb}_2\text{O}_5$  is composed of  $3 \times 5$  and  $3 \times 4$  metal–oxygen octahedra with the  $\text{ReO}_3$ -type structure<sup>21,22</sup>. These blocks are connected to the neighbouring blocks via edge-sharing; thus, the resulting crystal contains a smaller number of oxygens than that in the pure  $\text{ReO}_3$ -type structure. The  $\text{WO}_3$  crystal has a typical  $\text{ReO}_3$ -type structure, which is also a basic structure of the  $\text{Nb}_2\text{O}_5$  crystal. It has been suggested that the TTB-type structure can be obtained from the  $\text{ReO}_3$ -type structure by rotating the four octahedra near the centre of the  $4 \times 4$  slabs by  $45^\circ$  (Fig. 4f)<sup>23</sup>. In fact, this assumption was supported by several TEM images, in which linear arrays of the TTB-type structures with two occupied pentagonal tunnels were detected in a  $\text{ReO}_3$ -type crystal<sup>11,18</sup>. Similar to the results of this study, these tunnels were mostly occupied by Nb ions, which could likely diffuse into the  $\text{WO}_3$  solid. Therefore, the suggested transformation appears to be plausible. However, it may not be realistic because such a solid-state reaction would involve the elimination of the edge-sharing octahedra of  $\text{H-Nb}_2\text{O}_5$  (high-temperature form) crystals and diffusion of large numbers of Nb atoms into  $\text{WO}_3$  regions. In addition, the vapour pressure of  $\text{WO}_3$  is relatively high at a reaction temperature of approximately 1600 K, as a result,  $\text{WO}_3$  will not be able to remain in the solid-state and will ultimately vaporise. Therefore, the new structures studied in this work could be formed through a solid-state reaction that likely involved a simultaneous diffusion of both Nb and W ions as well as oxygen atoms.

## Methods

**Specimens.** The studied sample was prepared by heating a mixture of  $\text{Nb}_2\text{O}_5$  and  $\text{WO}_3$  compounds (their nominal compositions were  $\text{Nb}_2\text{O}_5:\text{WO}_3 = 19:63$ ) in a platinum-sealed capsule at 1620 K for 18 h with the subsequent quenching to maintain their high-temperature crystalline forms. The product obtained during a solid-state reaction contained a powder with a light grey colour and was identical to the specimen examined previously by one of the authors back in the 1970s<sup>11,17,18</sup>. The specimen has been provided by A. D. Wadsley and R. S. Roth and has been a part of a series of preparation used to identify the phases present in the  $\text{Nb}_2\text{O}_5\text{–WO}_3$  system<sup>24</sup>. A drop of the produced suspension was placed onto a holey carbon grid for microscopic observation, and thin portions of the produced sample flakes were examined at the direction of the incident electron beam parallel to the  $c$ -axis.

**Scanning transmission electron microscopy and energy-dispersive X-ray spectroscopy.** Two STEM-EDS electron microscopes were used in the present work.

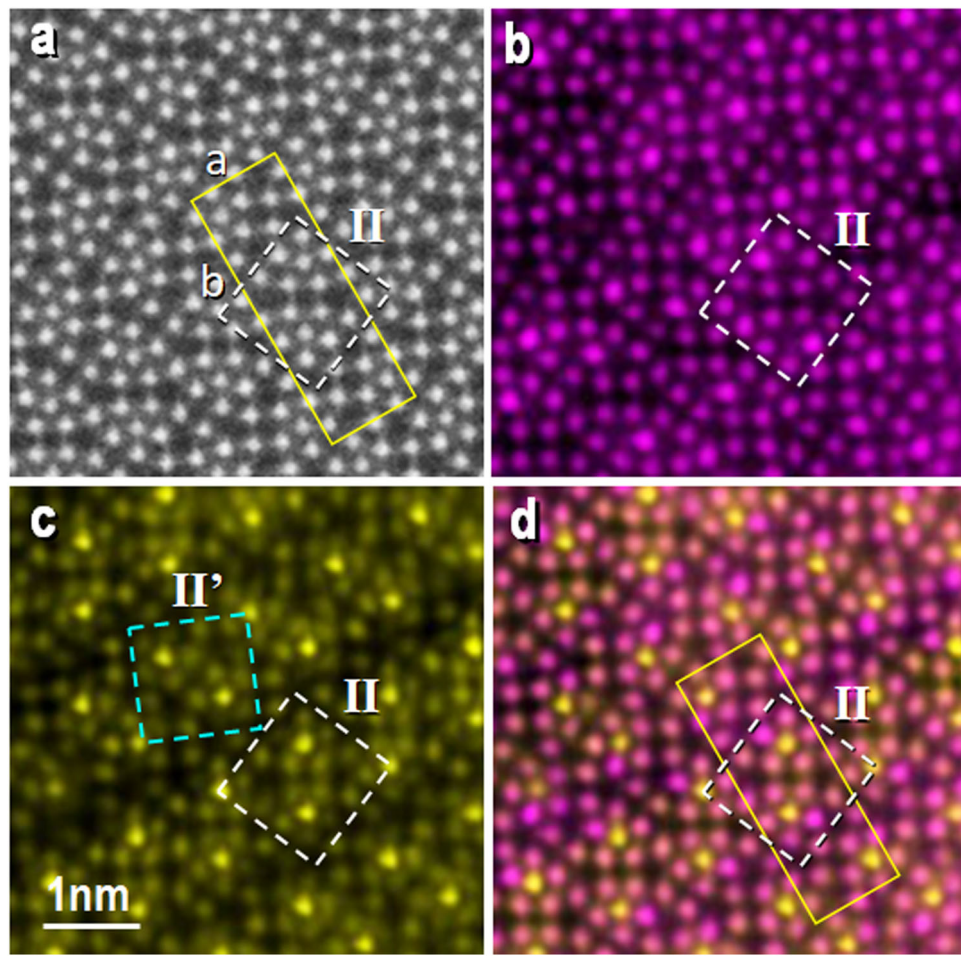


**Fig. 6 Three different types of the pentagonal tunnels present in the TTB-type units of the 2:7 and the 4:9 crystal structures.** **a, b** STEM-EDS images of the overlay images of W and Nb emissions for the 4:9 and the 2:7 crystals reproduced from Fig. 5b, d, respectively. The pentagonal tunnels are indicated by the dotted lines and denoted in panel **(c)** as A-C. The type A pentagons are deformed, while the other two types, B and C, appear to have the regular pentagonal shapes. The deformation of the pentagon consisting of octahedral rings in the TTB unit with the fully open tunnels is always associated with the existence of octahedral pairs containing Nb-richest (#1) and W-richest (#8) sites.

The first system consisting of a JEM-ARM200F microscope and two silicon drift detectors (SDDs) equipped with 100-mm<sup>2</sup> sensors were utilised to examine 4:9 crystals at an accelerating voltage of 200 kV. The second system operated at 300 kV included a JEM-ARM300F microscope and two SDDs equipped with 158-mm<sup>2</sup> sensors. This instrument was used to study 2:7 crystals. The noise levels in the EDS images obtained by the JEM-ARM200F instrument and 100-mm<sup>2</sup> SDDs were reduced by employing the Poisson nonlocal principal component analysis algorithm<sup>25</sup>.

#### Data availability

All data and detailed experiments are available from the corresponding author upon request.

Received: 5 October 2020; Accepted: 21 January 2021;

Published online: 01 March 2021

#### References

1. Iijima, S. High-resolution electron microscopy of crystal lattice of titanium-niobium oxides. *J. Appl. Phys.* **42**, 5891–5893 (1971).
2. Williams, D. B. & Carter, C. B. *Transmission Electron Microscopy*. (Published by Plenum Press, New York, 1996).
3. Suenaga, K. et al. Element-selective single atom imaging. *Science* **290**, 2280–2282 (2000).
4. Suenaga, K., Okazaki, T., Okunishi, E. & Matsumura, S. Detection of photons emitted from single erbium atoms in energy-dispersive X-ray spectroscopy. *Nat. Photonics* **6**, 545–548 (2012).
5. Shibata, N. et al. Atomic-scale imaging of individual dopant atoms in a buried interface. *Nat. Mater.* **8**, 654–658 (2009).
6. Feng, B. et al. Atomically ordered solute segregation behaviour in an oxide grain boundary. *Nat. Commun.* **7**, 11079 (2016).
7. Wenner, S., Jones, L., Marioara, C. D. & Holmestad, R. Atomic-resolution chemical mapping of ordered precipitates in Al alloys using energy-dispersive X-ray spectroscopy. *Microsc.* **96**, 103–111 (2017).
8. Yang, W. et al. Atom locations in a Ni doped  $\eta$ -(Cu,Ni)<sub>6</sub>Sn<sub>5</sub> intermetallic compound. *Scr. Mater.* **158**, 1–5 (2019).
9. Griffith, K. J. et al. Niobium tungsten oxides for high-rate lithium ion energy storage. *Nature* **559**, 556–563 (2018).
10. Yan, L. et al. Recent advances in nanostructured Nb-based oxides for electrochemical energy storage. *Nanoscale* **8**, 8443–8465 (2016).
11. Iijima, S. Structural studies by high-resolution electron microscopy: intergrowth of ReO<sub>3</sub>- and tetragonal tungsten bronze-type structures in the system Nb<sub>2</sub>O<sub>5</sub>-WO<sub>3</sub>. *Acta Cryst. A* **34**, 922–931 (1978).
12. Koçer, C. P., Griffith, K. J., Grey, C. P. & Morris, A. J. Cation disorder and lithium insertion mechanism of Wadsley-Roth crystallographic shear phases from first principles. *J. Am. Chem. Soc.* **141**, 15121–15134 (2019).
13. Heinrich, C. P. et al. Tetragonal tungsten bronzes Nb<sub>8-x</sub>W<sub>9+x</sub>O<sub>47-δ</sub>: optimization strategies and transport properties of a new n-type thermoelectric oxide. *Mater. Horiz.* **2**, 519–527 (2015).
14. Von Dreele, R. B. & Cheetham, A. K. The structures of some titanium-niobium oxides by powder neutron diffraction. *Proc. R. Soc. Lond. A.* **338**, 311–326 (1974).
15. Sleight, S. A. The crystal structure of Nb<sub>16</sub>W<sub>18</sub>O<sub>94</sub>, a member of (MeO)<sub>x</sub>MeO<sub>3</sub> family of compounds. *Acta Chem. Scand.* **20**, 1102–1112 (1996).
16. Krumeich, F. Order and disorder in niobium tungsten oxides of the tetragonal tungsten bronze type. *Acta Cryst. B* **54**, 240–249 (1998).

17. Iijima, S. & Alpress, J. G. Structural studies by high-resolution electron microscopy: tetragonal tungsten bronze-type structures in the system  $\text{Nb}_2\text{O}_5$ - $\text{WO}_3$ . *Acta Cryst.* **A30**, 22–29 (1974).
18. Iijima, S. & Alpress, J. G. Structural studies by electron microscopy: coherent intergrowth of the  $\text{ReO}_3$  and tetragonal tungsten bronze structure types in the system  $\text{Nb}_2\text{O}_5$ - $\text{WO}_3$ . *Acta Cryst.* **A30**, 29–36 (1974).
19. Stephenson, N. C. A structural investigation of some stable phases in the region  $\text{Nb}_2\text{O}_5$ - $\text{WO}_3$ - $\text{Nb}_3\text{O}_5$ . *Acta Cryst.* **B24**, 637–653 (1968).
20. Sena, R. P. et al. A pseudo-tetragonal tungsten bronze superstructure: a combined solution of the crystal structure of  $\text{K}_{6.4}(\text{Nb}, \text{Ta})_{36.3}\text{O}_{94}$  with advanced transmission electron microscopy and neutron diffraction. *Dalton Trans.* **45**, 973–979 (2016).
21. Iijima, S. Direct observation of lattice defects in  $\text{H-Nb}_2\text{O}_5$  by high-resolution electron microscopy. *Acta Cryst.* **A29**, 18–24 (1973).
22. Gatehouse, B. M. & Wadsley, A. D. The crystal structure of the high temperature form of niobium pentoxide. *Acta Cryst.* **17**, 1545–1554 (1965).
23. Hyde, B. G. & O'Keeffe, M. Relations between the  $\text{DO}_9(\text{ReO}_3)$  structure type and some 'bronze' and 'tunnel' structures. *Acta Cryst.* **A29**, 243–248 (1973).
24. Roth, R. S. & Wadsley, A. D. Multiple phases formation in binary system  $\text{Nb}_2\text{O}_5$ - $\text{WO}_3$ . I. Preparation and identification of phases. *Acta Cryst.* **19**, 26–32 (1965).
25. Harmany, S. Z., Deledalle, C. A. & Willett, R. Poisson noise reduction with non-local PCA. *J. Math. Imaging Vis.* **48**, 279–294 (2014).

## Acknowledgements

S.I. would like to thank Dr. T. Yumura for his useful discussion on the stability of the 4:9 crystals in terms of DFT calculations which will be published soon.

## Author contributions

I.O. conducted STEM-EDS experiments on the specimens of  $2\text{Nb}_2\text{O}_5\text{-}7\text{WO}_3$  oxides and W.Y. and S. Matsumura on  $4\text{Nb}_2\text{O}_5\text{-}9\text{WO}_3$  oxides. S.I. conceived the idea and analysed the data, and wrote the paper.

## Competing interests

The authors declare no competing interests.

## Additional information

**Supplementary information** The online version contains supplementary material available at <https://doi.org/10.1038/s43246-021-00128-z>.

**Correspondence** and requests for materials should be addressed to S.I.

**Peer review information** Primary handling editor: Aldo Isidori

**Reprints and permission information** is available at <http://www.nature.com/reprints>

**Publisher's note** Springer Nature remains neutral with regard to jurisdictional claims in published maps and institutional affiliations.



**Open Access** This article is licensed under a Creative Commons Attribution 4.0 International License, which permits use, sharing, adaptation, distribution and reproduction in any medium or format, as long as you give appropriate credit to the original author(s) and the source, provide a link to the Creative Commons license, and indicate if changes were made. The images or other third party material in this article are included in the article's Creative Commons license, unless indicated otherwise in a credit line to the material. If material is not included in the article's Creative Commons license and your intended use is not permitted by statutory regulation or exceeds the permitted use, you will need to obtain permission directly from the copyright holder. To view a copy of this license, visit <http://creativecommons.org/licenses/by/4.0/>.

© The Author(s) 2021